Ab initio interionic potentials for NaCl by multiple lattice inversion

Shuo Zhang and Nanxian Chen

Department of Physics, Tsinghua University, Beijing 100084, China
and Institute for Applied Physics, University of Science and Technology, Beijing 100083, China
(Received 27 November 2001; revised manuscript received 1 March 2002; published 14 August 2002)

Based on the Chen-Möbius lattice inversion and a series of pseudopotential total-energy curves, a different method is presented to derive the *ab initio* interionic pair potentials for $B1$-type ionic crystals. Comparing with the experimental data, the static properties of $B1$- and $B2$-type NaCl are well reproduced by the interionic potentials. Moreover, the phase stability of $B1$-NaCl has been described by the energy minimizations from the global deformed and disturbed states. The molecular-dynamics simulations for the molten NaCl indicate that the calculated mean-square displacements, radial distribution function, and diffusion coefficients gain good agreements with the experimental results. It can be concluded that the inversion pair potentials are valid over a wide range of interionic separations for describing the structural properties of $B1$-type ionic crystals.

I. INTRODUCTION

With the development of computational techniques, the atomistic modeling techniques are now used extensively in investigating the properties and behaviors of ionic materials.[1-3] Although these properties could be obtained from *ab initio* calculations,[4] it is very costly for large-scale simulations, especially for the systems containing more than hundreds of ions. This consequently highlights the applications of interionic potentials,[5-8] which allow fast simulations for large ionic systems. However, the success of atomistic simulations is mainly dependent on the validity of interionic potentials. In the previous work,[5,9-11] the *a priori* interionic potential functions were often predetermined for both of short-range and long-range interactions, respectively; and the adjustable parameters in potentials were obtained from the equilibrium and near-equilibrium properties. This might lead to the question how to avoid the *a priori* potential functions and define the ionic charges correctly.

This question motivated the present work. A different parameter-free method for interionic potentials could be presented as follows. First, taking NaCl as a prototypical system, we constructed the extended phase space including $B1$ (rocksalt) and three related structures. The aim was to derive the proper interionic potentials from an extended phase space including equilibrium and nonequilibrium states. This could cover more configurations and interionic spacings of our interest than that only from one equilibrium configuration.[12] Second, the pseudopotential total-energy calculations for four-type NaCl crystals were performed from lattice constant $a = 4.5 - 16.0$ Å. Third, at larger lattice constant a, the effective charges on ions were determined by fitting to the total-energy difference between $B1$ and one of the related structures ($B3$ zinc blende), instead of the formal or Mulliken charges as in convention. Finally, the short-range pair potential curves were directly evaluated from a sreies of the total-energy difference based on Chen-Möbius lattice inversion techniques.[13,14] Then the suitable functions forms were selected to fit the pair potential curves. Furthermore, these inverted pair potentials were used to describe the properties of

NaCl in $B1$, $B2$, disordered and molten states, and the validity of present potentials has been discussed in detail.

II. COMPUTATIONAL MODELS

In terms of the descriptions of pair potentials,[15] the total-energy $E_{\text{tot}}^{B1}(a)$ of $B1$-NaCl at lattice constant a can be expressed as Eq. (1), which includes three kinds of ionic interactions $E_{\text{Na-Cl}}^{B1}(a)$, $E_{\text{Na-Na}}^{\text{fcc}}(a)$, and $E_{\text{Cl-Cl}}^{\text{fcc}}(a)$,

$$E_{\text{tot}}^{B1}(a) = E_{\text{Na-Cl}}^{B1}(a) + E_{\text{Na-Na}}^{\text{fcc}}(a) + E_{\text{Cl-Cl}}^{\text{fcc}}(a) + E_{\text{iso}}, \quad (1)$$

where the $E_{\text{Na-Na}}^{\text{fcc}}(a)$ and $E_{\text{Cl-Cl}}^{\text{fcc}}(a)$ are the like-ion contributions on fcc (face-centered-cubic) sublattice, E_{iso} is the energy of isolated ions, which is independent on the interionic separation. Only with the $E_{\text{tot}}^{B1}(a)$, we cannot separately calculate each item of the right side in Eq. (1), so three other virtual structures are introduced with regard to $B1$, which may not exist in nature. Their *ab initio* total energies could be calculated for a series of lattice constant a.[16] Based on the differences between these total energies, the partial lattice energy as a function of only one kind of interionic pair potential can be obtained. It is worth noting that the virtual structures should be constructed properly. For example, in order to derive the Na-Cl pair potential, if a Na fcc and a Cl fcc lattices constitute a $B3$-NaCl, its total energy is

$$E_{\text{tot}}^{B3}(a) = E_{\text{Na-Cl}}^{B3}(a) + E_{\text{Na-Na}}^{\text{fcc}}(a) + E_{\text{Cl-Cl}}^{\text{fcc}}(a) + E_{\text{iso}}, \quad (2)$$

with the identical lattice constant a, the difference between $B1$ and $B3$ structures is only the relative displacement of cation and anion sublattices. From $B1$ to $B3$, the Na-Na and Cl-Cl distances are unaffected by this displacement, and their total-energy difference is only about the Na-Cl interactions and can be expressed as

$$\Delta E_{\text{Na-Cl}}(a) = E_{\text{tot}}^{B1}(a) - E_{\text{tot}}^{B3}(a) = E_{\text{Na-Cl}}^{B1}(a) - E_{\text{Na-Cl}}^{B3}(a). \quad (3)$$

Then the Na-Cl pair potential curve can be evaluated by lattice inversion.[13,14] However, if the $B2$ (CsCl-type) model is selected, from $B1$ to $B2$, the Na-Cl, Na-Na, and Cl-Cl
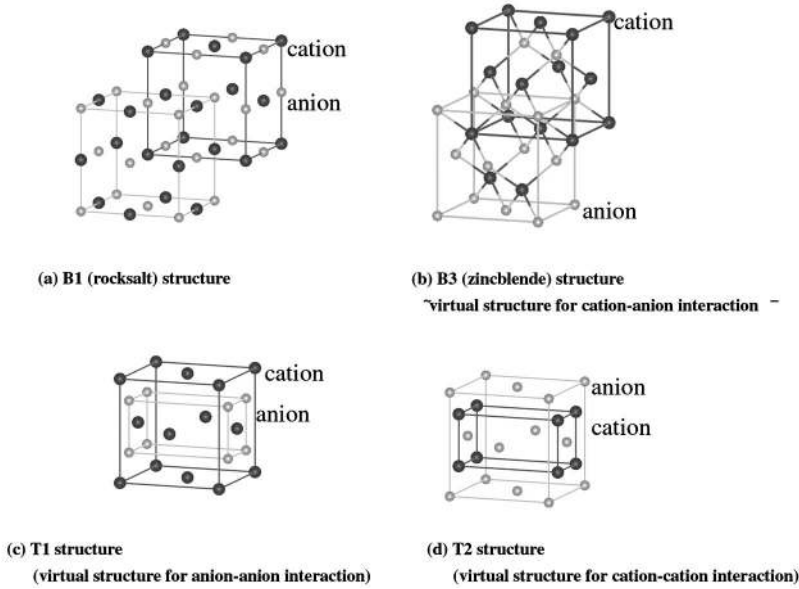
FIG. 1. Virtual structures used for *ab initio* pseudopotential total-energy calculations. (a) $B1$ (rocksalt) structure; (b) $B3$ (zinc blende) structure (virtual structure for cation-anion interaction); (c) $T1$ structure (virtual structure for anion-anion interaction); (d) $T2$ structure (virtual structure for cation-cation interaction).

interactions all undergo changes because cations and anions in the $B2$ structure are placed on the sc (simple cubic) sublattices. Therefore the combination of $B1$ and $B2$ structures could not give more information than the single $B1$ or $B2$ structure.

In order to obtain the Cl-Cl interaction from the total energies, the $T1$ structure is built as shown in Fig. 1(c), which consists of a cation fcc and an anion tetragonal sublattice. Its total energy can be expressed as

$$E_{\text{tot}}^{T1}(a) = E_{\text{Na-Cl}}^{T1}(a) + E_{\text{Na-Na}}^{\text{fcc}}(a) + E_{\text{Cl-Cl}}^{\text{tetra}}(a) + E_{\text{iso}}. \quad (4)$$

For $B1$- and $T1$-NaCl at the same lattice constant a, their cation-cation interaction $E_{\text{Na-Na}}^{\text{fcc}}(a)$ and $E_{\text{Na-Na}}^{\text{fcc}}(a)$ are identical, and their contributions from unlike-ion interactions can be separately calculated by the above Na-Cl pair potential. Hence the partial lattice energy as a function of the Cl-Cl pair potential can be derived from the total-energy difference between $B1$-and $T1$-NaCl.

As for the cation-cation interaction, the $T2$ structure is generated by exchanging the atomic sites of cations and anions in the $T1$ structure. The $T1$ and $T2$ structures have the identical space group $P4/mmm$. Then the total energy of $T2$-NaCl is

$$E_{\text{tot}}^{T2}(a) = E_{\text{Na-Cl}}^{T2}(a) + E_{\text{Na-Na}}^{\text{tetra}}(a) + E_{\text{Cl-Cl}}^{\text{fcc}}(a) + E_{\text{iso}}. \quad (5)$$

Similarly, the Na-Na partial lattice energy can also be obtained from the total-energy difference between $B1$- and $T2$-NaCl.

As for the total energies of NaCl crystals in $B1$, $B3$, $T1$, and $T2$ structures, they were calculated by using the GGA (generalized gradient approximations) implemented in the CASTEP program.[17–19] The ultrasoft pseudopotentials for Na and Cl were used in this work. A plane-wave basis set with 410-eV cutoff was applied. The k-mesh points over the Brillouin zone were generated with parameters $4 \times 4 \times 4$ for the biggest reciprocal space and $1 \times 1 \times 1$ for the smallest one by the Monkhorst-Pack-scheme[20] corresponding to the lattice

constant a. The energy tolerance for self-consistent field (SCF) convergence was 2×10^{-6} eV/atom for all calculations. Figure 2 shows the calculated total energies of $B1$-, $B3$-, $T1$-, and $T2$-type NaCl crystals as a function of crystal lattice constant a.

III. DERIVATION OF INTERIONIC POTENTIALS FOR NaCl

A. Na-Cl interionic potential

According to Eq. (3), the total-energy difference between $B1$- and $B3$-NaCl only depends on the Na-Cl interaction, and can be rewritten as

$$\Delta E_{\text{Na-Cl}}(a) = \Delta E_{\text{Na-Cl}}^{\text{Coul}}(a) + \Delta E_{\text{Na-Cl}}^{\text{SR}}(a), \quad (6)$$

in which $\Delta E_{\text{Na-Cl}}^{\text{SR}}(a)$ is the short-range interaction, and $\Delta E_{\text{Na-Cl}}^{\text{Coul}}(a)$ is the long-range Coulomb part. For $B1$- and $B3$-NaCl, their Coulomb part are treated as follows. First, the ionic interaction can be approximately devoted only by Coulomb potential at larger interionic separation. And the
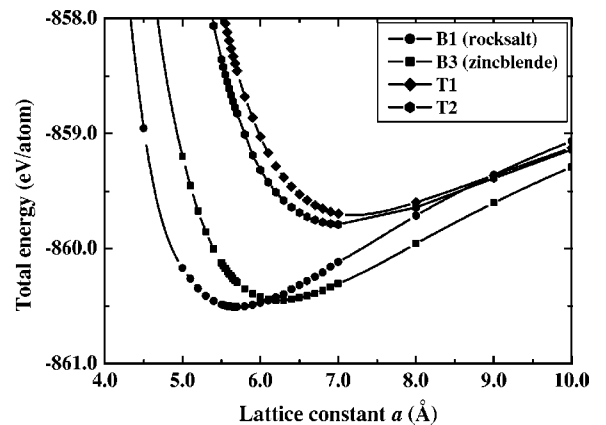

FIG. 2. NaCl total energies vs lattice constant a in different virtual structures from *ab initio* pseudopotential calculations.
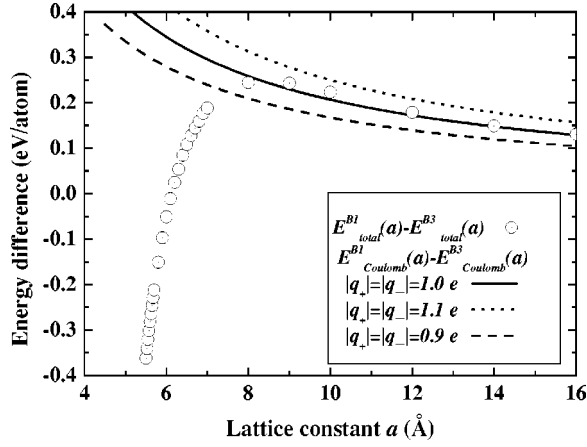
FIG. 3. The total-energy and Coulomb interaction differences between $B1$ and $B3$ NaCl vs lattice constant a.

Coulomb interaction can be calculated by the fixed effective charges over a wide range of interionic distances. Second, in order to estimate the effective charges on ions, the pseudopotential total-energy calculations were extended to the lattice constant $a=16.0$ Å for $B1$- and $B3$-NaCl. When $a \geqslant 8.0$ Å, their lattice energies are approximatively regarded as only the sum of Coulomb potential, then we get

$$E_{\text{tot}}^{B1}(a) - E_{\text{tot}}^{B3}(a) = E_{\text{Coul}}^{B1}(a) - E_{\text{Coul}}^{B3}(a). \tag{7}$$

By using Coulomb potential to fit the total-energy difference between $B1$- and $B3$-NaCl at larger lattice constant a, the effective ionic charges can be estimated as shown in Fig. 3. During the fitting, the Coulomb interactions can be evaluated by Ewald summation technique.[21] It can be seen that the calculated ionic charges are exactly coincident with the full ionic charges for NaCl.

After the determination of effective charges q_+ and q_-, the short-range interaction difference between $B1$- and $B3$-NaCl is

$$\Delta E_{\text{Na-Cl}}^{\text{SR}}(a) = E_{\text{Na-Cl(SR)}}^{B1}(a) - E_{\text{Na-Cl(SR)}}^{B3}(a)$$
$$= E_{\text{tot}}^{B1}(a) - E_{\text{Coul}}^{B1}(a) + E_{\text{tot}}^{B3}(a) - E_{\text{Coul}}^{B3}(a). \tag{8}$$

For the $B1$-type NaCl, the short-range Na-Cl interaction per ion can be expressed as

$$E_{\text{Na-Cl(SR)}}^{B1}(a)$$
$$= \frac{1}{2} \sum_{i,j,k} \phi_{\text{Na-Cl}}^{\text{SR}}$$
$$\times \left(\sqrt{(i+k-1)^2 + (i+j-1)^2 + (j+k-1)^2} \frac{a}{2} \right), \tag{9}$$

where the $\phi_{\text{Na-Cl}}^{\text{SR}}$ is the Na-Cl short-range pair potential, the i, j, k indicate the atomic sites of ions in the unit of the lattice constant a. In the B3-NaCl, the Na-Cl short-range interaction per ion is
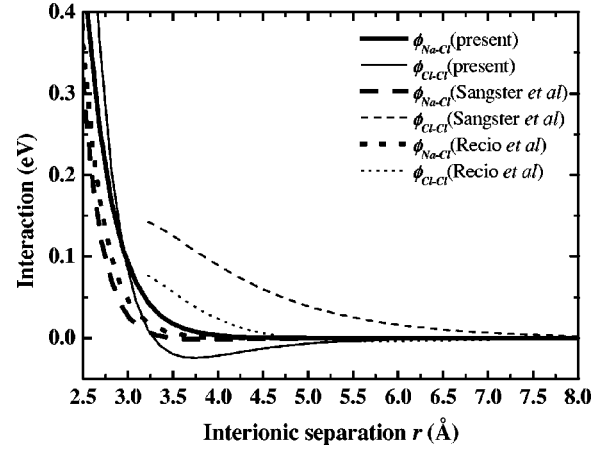

FIG. 4. Short-range interionic potentials for NaCl.

$$E_{\text{Na-Cl(SR)}}^{B3}(a)$$
$$= \frac{1}{2} \sum_{i,j,k} \phi_{\text{Na-Cl}}^{\text{SR}}$$
$$\times \left(\sqrt{\left(i+k-\frac{1}{2}\right)^2 + \left(i+j-\frac{1}{2}\right)^2 + \left(j+k-\frac{1}{2}\right)^2} \frac{a}{2} \right). \tag{10}$$

Thus, based on the Chen-Möbius lattice inversion,[13,14] the interaction $\Delta E_{\text{Na-Cl}}^{\text{SR}}(x)$ per ion can be expressed as the form as follows:

$$\Delta E_{\text{Na-Cl}}^{\text{SR}}(x) = \frac{1}{2} \sum_n r_0(n) \phi_{\text{Na-Cl}}^{\text{SR}}[b_0(n)x], \tag{11}$$

where x is the nearest-neighbor distance, $b_0(n)x$ is the nth-neighbor distance, and $r_0(n)$ is the nth coordination number. The series $\{b_0(n)\}$ is extended into a multiplicative semigroup. Then for any two integers m and n, there always exists an integer k such that

$$b(k) = b(m)b(n). \tag{12}$$

The $\Delta E_{\text{Na-Cl}}^{\text{SR}}(x)$ can be rewritten as

$$\Delta E_{\text{Na-Cl}}^{\text{SR}}(x) = \frac{1}{2} \sum_n r(n) \phi_{\text{Na-Cl}}^{\text{SR}}[b(n)x], \tag{13}$$

where

$$r(n) = \begin{cases} r_0(b_0^{-1}[b(n)]) & \text{if } b(n) \in \{b_0(n)\} \\ 0 & \text{if } b(n) \notin \{b_0(n)\} \end{cases}. \tag{14}$$

Thus the pair potentials $\phi_{\text{Na-Cl}}^{\text{SR}}$ between Na and Cl ions can be expressed as

$$\phi_{\text{Na-Cl}}^{\text{SR}}(x) = 2 \sum_{n=1}^{\infty} I(n) \Delta E_{\text{Na-Cl}}^{\text{SR}}[b(n)x], \tag{15}$$

in which the inversion coefficient $I(n)$ is given by

TABLE I. Interionic parameters derived by lattice inversion in this work. The short-range terms are truncated at the value of $r_c = 12.00$ Å.

Na-Cl			Cl-Cl			Coulomb	
D_{+-} (eV)	R_{+-} (Å)	γ_{+-}	D_{--} (eV)	R_{--} (Å)	γ_{--}	q_+	q_-
0.284 75	2.649 88	8.672 92	0.024 36	3.733 82	11.390 17	$+e$	$-e$

$$\sum_{b(n)/b(k)} I(n) r\left[b^{-1}\left(\frac{b(k)}{b(n)} \right) \right] = \delta_{k1}, \qquad (16)$$

then the short-range Na-Cl pair potential curve is obtained from lattice inversion as shown in Fig. 4. The shape of pair potential curve indicates the repulsive exponential function form is suitable to express the Na-Cl short-range interaction, and then the total Na-Cl pair potential is

$$\Phi_{\text{Na-Cl}-}(r) = \phi_{\text{Na-Cl}-}^{\text{SR}}(r) + \phi_{\text{Na-Cl}-}^{\text{Coul}}(r)$$

$$= D_{+-} \exp\left[\gamma_{+-}\left(1 - \frac{r}{R_{+-}} \right) \right] + \frac{q_+ q_-}{4\pi\varepsilon_0 r}. \qquad (17)$$

B. Cl-Cl interionic potential

Using the above inverted Na-Cl pair potential, we can calculate the Na-Cl interaction in $B1$- and $T1$-NaCl crystals, respectively. Then the short-range Cl-Cl interaction difference between $B1$- and $T1$-NaCl is obtained by

$$\Delta E_{\text{Cl-Cl}}^{\text{SR}}(a) = E_{\text{Cl-Cl(SR)}}^{B1}(a) - E_{\text{Cl-Cl(SR)}}^{T1}(a)$$

$$= E_{\text{tot}}^{B1}(a) - E_{\text{Coul}}^{B1}(a) - E_{\text{Na-Cl(SR)}}^{B1}(a)$$

$$+ E_{\text{tot}}^{T1}(a) - E_{\text{Coul}}^{T1} - E_{\text{Na-Cl(SR)}}^{T1}(a). \qquad (18)$$

The Cl-Cl short-range interaction per ion in $B1$-NaCl can be expressed as

$$E_{\text{Cl-Cl(SR)}}^{B1}(a)$$

$$= \frac{1}{4} \sum_{i,j,k \neq 0} \phi_{\text{Cl-Cl}}\left(\sqrt{(i+j)^2 + (i+k)^2 + (j+k)^2}\,\frac{a}{2} \right). \qquad (19)$$

In the $T1$ structure, the Na-Cl and Cl-Cl short-range interactions are separately defined as follows:

$$E_{\text{Na-Cl(SR)}}^{T1}(a)$$

$$= \frac{1}{2} \sum_{i,j,k} \phi_{\text{Na-Cl}}^{\text{SR}}$$

$$\times \left(\sqrt{\left(i+k-\frac{1}{2} \right)^2 + \left(i+j-\frac{1}{2} \right)^2 + (j+k)^2}\,\frac{a}{2} \right), \quad (20)$$

$$E_{\text{Cl-Cl(SR)}}^{T1}(a) = \frac{1}{4} \sum_{i,j,k \neq 0} \phi_{\text{Cl-Cl}}^{\text{SR}}\left(\sqrt{i^2 + 4j^2 + k^2}\,\frac{a}{2} \right). \qquad (21)$$

By Chen-Möbius lattice inversion, the Cl-Cl short-range potential is calculated as Fig. 4. In terms of the curve shape, a Morse-stretch function form is selected for Cl-Cl short-range potential, and finally the Cl-Cl pair potentials is

$$\Phi_{\text{Cl-Cl}}(r)$$

$$= D_{--}\left(\left\{ 1 - \exp\left[\gamma_{--}\left(1 - \frac{r}{R_{--}} \right) \right] \right\}^2 - 1 \right) + \frac{q_- q_-}{4\pi\varepsilon_0 r}. \qquad (22)$$

C. Na-Na pair potential

By the similar method for Cl-Cl pair potential, the Na-Na pair potential can also be obtained. Based on our calculations, the short-range interaction between Na ions is very small and can be neglected, thus the Na-Na interaction can be expressed only by Coulomb potential,

$$\Phi_{\text{Na-Na}}(r) = \frac{q_+ q_+}{4\pi\varepsilon_0 r}. \qquad (23)$$

Finally, all the potential parameters have been obtained as given in Table I.

IV. APPLICATION OF INTERIONIC POTENTIALS

A. Static properties of NaCl crystal

Using the above interionic potentials from multiple lattice inversion, we first calculated the static properties of equilibrium $B1$-NaCl at zero temperature and pressure, as shown in Table II.

By comparison, the lattice constants, lattice energy, and elastic properties have also been calculated based on the Recio's *ab initio* interionic potentials,[22] COMPASS Forcefield,[24] and Gorden-Kim electron-gas model,[25] respectively. The results are also listed in Table II. From the short-range potential curves in Fig. 4, it is obvious that present potentials are different from that of other previous works,[23,22] especially the Cl-Cl pair potential. At the Cl-Cl nearest distance 3.96 Å, the Sangster's empirical[23] and Recio's *ab initio* potentials[22] are both repulsive, and ours is slightly attractive. Despite the difference, the present potentials still well reproduce the equilibrium lattice parameters, bulk modulus, elastic constants, and lattice energy as the previous potentials, which are in good agreement with experimental data.[26]

Besides the static properties of $B1$-NaCl, another important test for the potential validity is to obtain the potentials from the properties of one phase of a material, and then to use them to calculate the properties of other phases. In this work we used the potentials from $B1$ and virtual structures to calculate the properties of $B2$ phase, while the $B2$ structure

TABLE II. The equilibrium lattice constant, elastic constants, and lattice energy of $B1$-NaCl calculated by different interionic potentials. Present work: lattice-inversion interionic potentials of this work; Recio's: *ab initio* pair potentials of Recio's work (Ref. 22); COMPASS: COMPASS Forcefield of MSI (Ref. 24); GK-ES: Gorden-Kim-type electron-gas potentials (Ref. 25). Experimental data (Ref. 26).

	Lattice constant a_0	Bulk modulus B_0 (GPa)	Lattice Energy $E_{lattice}$ (eV)	Elastic constants (GPa)		
				C_{11}	C_{12}	C_{44}
Present work	5.610	28.64	8.09	58.43	13.73	13.73
Recio's	5.540	32.93	8.27	67.29	15.74	15.74
COMPASS	5.643	33.11	8.15	60.35	19.49	19.49
GK-ES	5.571	28.08	7.97			
Experiment	5.640	28.50	8.04	60.00	12.70	14.00

has not been used in the potential derivation. For comparison, the properties of $B2$-NaCl have also been calculated based on the previous potentials. All results are shown in Table III.

The values in Table III reveal that present potential produced the consistent results with that of COMPASS Forcefield[24] and Gorden-Kim electron-gas model,[25] and a little difference from that of Recio's.[22] All calculated values are very close to the experimental data.[27] This shows that present interionic potentials have good transferability between $B1$ and $B2$ phases. The reason may be that our potentials were derived from the $B1$ and its related virtual structures, and this covers more configurations of phase space. Hence, despite that the $B2$ was not involved in the potential derivation, the potentials still well reproduce the properties of $B2$-NaCl. From $B1$ to $B2$, this successful transferability implies the advantages of potentials from the extended phase space.

B. Stability of $B1$-NaCl crystal

Unlike most previous potentials,[22–25] we took the structural stability as an important test for the present potentials. As a set of effective potentials, we think, the corresponding interionic forces should make the deformed structures recover to the equilibrium phase with the lowest energy. So based on the present interionic potentials, the energy minimization for deformed $B1$-NaCl were performed by the conjugated gradient algorithm.

The detail of lattice deformation is described in Table IV. The deformed structures were constructed by randomly setting the lattice parameters, for example, the lattice constant a

is from $0.36a_0$ to $1.78a_0$ (a_0 is the equilibrium lattice constant), the axial angle is even inclined to 30°, and some initial structures are constructed by simultaneously changing the lattice constants and axial angles. With the ten deformed $B1$-NaCl's listed in Table IV, their energy minimizations were performed to search the stable configurations from these initial configurations.

After the energy minimizations, the final relaxed structures show that COMPASS, Recio's and our potentials all exhibited good abilities for describing the stability of $B1$-NaCl, as shown in Table IV. Only several deformed structures could not returned to the equilibrium $B1$-NaCl based on COMPASS or Recio's potentials. The reason might be their potentials were used beyond their valid ranges in our calculations, and led to some collapsed lattices. Nevertheless, this test suggests that the present potentials appears promising in describing the stability of the NaCl crystal.

As the further test for the structural stability, the lattice energies of NaCl in five typical AB-type binary structures, $B1$ (rocksalt), $B2$ (CsCl-type), $B3$ (zinc blende), $B8_1$ (NiAs-type) and $L1_0$ (CuAu-type) were also evaluated in this work. The results are shown in Fig. 5. In order to make the comparison, these calculations have also been done by the Recio's potentials and pseudopotential method implemented in CASTEP. All calculations show the similar trends that the energy of equilibrium $B1$ phase is the lowest. This may explain the stability of rocksalt NaCl under normal temperature and pressure. Besides, the Fig. 5 also shows the $B1$ phase becomes less stable than $B2$ phase with the cell volume decreasing. Consequently, this can be an important reason for the $B1 \rightarrow B2$ transition of NaCl under high pressure. It is

TABLE III. Static properties of $B2$-NaCl at zero temperature and pressure calculated by several interionic potentials.

	Lattice constant a_0 (Å)	Bulk modulus B_0 (GPa)	Lattice energy $E_{lattice}$ (eV)	Volume at 0 Pa V_0 (Å^3)
Present work	3.407	33.47	7.85	39.55
Recio's (Ref. 22)	3.287	37.79	8.06	35.51
COMPASS (Ref. 24)	3.498	33.24	7.68	42.80
GK-ES (Ref. 25)	3.420	37.31	7.67	41.00
Expt (Ref. 27)	3.469	36.20		41.73

TABLE IV. Energy minimization results from the initial deformed to the final stable structures based on different interionic potentials in which the lattice parameters are in the units of their equilibrium values a_0, b_0, c_0, α_0, β_0, and γ_0.

Initial (unrelaxed) a/a_0, b/b_0, c/c_0	α/α_0, β/β_0, γ/γ_0	Interionic potentials	Final (relaxed) a/a_0, b/b_0, c/c_0	α/α_0, β/β_0, γ/γ_0
0.36, 100, 1.00	1.00, 1.00, 1.00	present work	1.00, 1.00, 1.00	1.00, 1.00, 1.00
		COMPASS	1.00, 1.00, 1.00	1.00, 1.00, 1.00
		Recio's	1.00, 1.00, 1.00	1.00, 1.00, 1.00
1.78, 1.00, 1.00	1.00, 1.00, 1.00	present work	1.00, 1.00, 1.00	1.00, 1.00, 1.00
		COMPASS	1.00, 1.00, 1.00	1.00, 1.00, 1.00
		Recio's	1.00, 1.00, 1.00	1.00, 1.00, 1.00
1.00, 1.00, 1.00	0.33, 1.00, 1.00	present work	1.00, 1.00, 1.00	1.00, 1.00, 1.00
		COMPASS	1.00, 1.00, 1.00	1.00, 1.00, 1.00
		Recio's	collapsed lattice	
0.36, 0.36, 0.36	0.66, 0.66, 0.66	present work	1.00, 1.00, 1.00	1.00, 1.00, 1.00
		COMPASS	1.00, 1.00, 1.00	1.00, 1.00, 1.00
		Recio's	collapsed lattice	
1.78, 1.78, 1.78	0.62, 0.62, 0.62	present work	1.00, 1.00, 1.00	1.00, 1.00, 1.00
		COMPASS	1.00, 1.00, 1.00	1.00, 1.00, 1.00
		Recio's	1.00, 1.00, 1.00	1.00, 1.00, 1.00
0.36, 1.07, 1.96	0.91, 0.83, 1.07	present work	1.00, 1.00, 1.00	1.00, 1.00, 1.00
		COMPASS	0.84, 0.99, 1.76	1.38, 1.00, 1.00
		Recio's	1.00, 1.00, 1.00	1.00, 1.00, 1.00
0.36, 0.36, 0.36	0.50, 0.62, 0.97	present work	1.00, 1.00, 1.00	1.00, 1.00, 1.00
		COMPASS	1.00, 1.00, 1.00	1.00, 1.00, 1.00
		Recio's	collapsed lattice	
0.54, 0.71, 0.89	0.56, 0.84, 1.22	present work	1.00, 1.00, 1.00	1.00, 1.00, 1.00
		COMPASS	1.00, 1.00, 1.73	0.61, 0.61, 1.00
		Recio's	1.00, 1.00, 1.73	0.61, 0.61, 1.00
1.78, 1.78, 0.90	0.92, 0.70, 0.95	present work	1.00, 1.00, 1.00	1.00, 1.00, 1.00
		COMPASS	2.44, 2.74, 0.89	1.00, 0.76, 0.99
		Recio's	1.00, 1.00, 1.00	1.00, 1.00, 1.00
1.43, 1.78, 0.72	0.80, 0.74, 1.07	present work	1.00, 1.00, 1.00	1.00, 1.00, 1.00
		COMPASS	1.00, 1.00, 1.00	1.00, 1.00, 1.00
		Recio's	1.00, 1.71, 1.00	1.39, 1.00, 1.39

seen in Fig. 5 that there are good agreements between the present potentials and CASTEP *ab initio* calculations, and the obvious differences exist between the Recio's potentials and CASTEP results. The main reason is that present potentials are derived from *ab initio* calculations of NaCl in multiple structures. Even the $B2$, $L1_0$, and $B8_1$ structures were not involved in the derivation of present potentials, the calculated lattice energies are still very close to those from *ab initio* calculations. Whereas the Recio's potentials were obtained only from the *ab initio* perturbed ion calculations for $B1$-NaCl, then the properties of NaCl in $B2$, $B3$, $L1_0$, and $B8_1$ structures might not be well described. This leads us to believe that the present method is more promising in the derivation of interionic potentials.

C. Transition from the disordered to ordered NaCl

Besides the interpretation of the structural stability, the present potentials were used to describe the transition from the disordered to the ordered states in NaCl. The disordered structure was built by randomly moving all ions 0.8 Å (28% of the nearest-neighbor distance) from their origin sites in a $B1$-type periodic supercell, which including 256 sodium ions and 256 chloride ions, as shown in Fig. 6(a). Comparison with the radial distribution functions (RDF's) of the disordered and molten NaCl,[28] this disordered NaCl, to some extent, could be considered as the molten NaCl like. Then based on the conjugated gradient algorithm, the energy minimization led to the transition from disordered to ordered NaCl, as shown from Figs. 6(a)–(e). The corresponding RDF's of intermediate configurations show how the disordered gradually changes into the ordered states. This transition may be considered as a special transition path from the molten NaCl to the solid. To our knowledge, it is very strict for the interionic potentials to make the disordered structure recover to the real equilibrium phase, especially the disordered phase is obtained by randomly moving all ions 0.8 Å from their equilibrium sites. Thus this transition indicates the present interionic potentials are valid over a wide range of interionic distance.
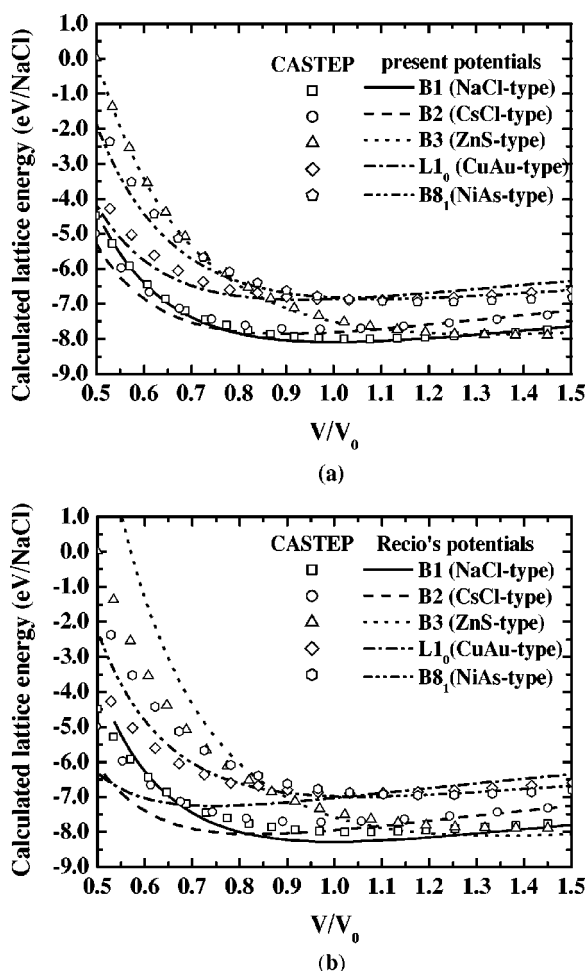
FIG. 5. Comparison of calculated lattice energies of NaCl in five typical *AB*-type binary structures: (a) present interionic potentials and CASTEP calculations, (b) Recio's interionic potentials and CASTEP calculations.

D. Molecular-dynamics simulations

The above relaxation for disordered NaCl suggests that the present potentials could be used to study the properties of molten NaCl. Then we performed the molecular dynamics (MD) simulations for $B1$-NaCl around the melting temperature $T = 1074$ K.[29] The MD cell was formed into a supercell with $5 \times 5 \times 5$ fcc unit cells, in which 1000 particles with 500 Na and 500 Cl ions were included. The initial configuration was to put the Na and Cl ions on the equilibrium sites of $B1$ lattice, corresponding to the lowest energy at zero temperature and pressure. The MD simulations were carried out for melting NaCl from 1000 to 1150 K at a step of 25 K, and for molten NaCl from 1200 to 1450 K at a step of 50 K. At each temperature, the calculations were performed for 20 000 time steps, where one time step was 2.0×10^{-15} s. The periodic boundary condition was applied and the Ewald sum method was used to take account of the Coulomb interaction. During the simulation, the constant-temperature, constant-pressure ensemble (N-P-T) was used to control both the temperature and pressure, and the extended system[30] with thermostat and barostat relaxation time of 0.1 ps adopted. The calculation for the initial 8000 time steps was used for stabilizing the

system and the data after 8000 time steps were used for deriving physical quantities of interest.

According to the MD simulations, the configurations corresponding to 1000, 1100, and 1200 K are depicted in the Fig. 7, respectively. These configurations provided the evidence of the melting in NaCl crystal. Before the melting point [Fig. 7(a)], all ions vibrated around their equilibrium sites. In spite of the large vibration amplitudes, the motion ions were strongly localized around their origin sites. At 1100 K, which is a little above the melting point $T = 1074$ K, some ions began to escape from their regular sites and diffused into the lattice interstitial positions. And other ions were still limited on the fcc lattice sites as shown in Fig. 7(b). With temperature further increasing, the diffusion of Na and Cl ions were so obvious that their origin sites could not be distinguished in Fig. 7(c) at 1200 K. This configuration suggests that NaCl has melted into the liquid. This may provide the atomistic pictures about the melting procedure of NaCl.

With the MD simulations, the variation of mean-square displacements MSD's near the melting point could also be calculated. As can be seen in Fig. 8, the ions drastically vibrated around their equilibrium positions at the temperature near to the melting point. But their diffusions were too slight to be observed because the slope of MSD ($T = 1050$ K) is almost zero. At the melting temperature, as shown by the solid line in Fig. 8, the slope of MSD increased with time, and this showed the start of melting. Above the melting point, the MSD's were obviously increasing with the time and temperature; this well described the self-diffusion of ions and the properties of molten salt. Hence, according to variations of MSD's at different temperatures, the melting temperature can be estimated as $T = 1075$ K, which is very close to the experimental data.[29]

From the MD simulations of molten NaCl at 1150 K, the Na-Cl radial distribution function (RDF) has also been calculated and compared with the those from COMPASS Force-field and experimental data.[31] The results show there is a good agreement among the present potentials, COMPASS, and experimental results. Especially, it is worth noting that the present RDF is obtained at temperature 1150 K, which is very close to the corresponding experimental temperature 1148 K (see Fig. 9). And the previous MD simulations were performed at 1073 K (Ref. 35) and 1427 K,[31,32] which are far from that of the experiments. This shows present potentials are more accuracy in the simulations for molten salt.

In terms of the calculated mean-square displacements MSD's of molten NaCl, we have also evaluated the self-diffusion coefficients from the inclination of the linear relation between MSD and time,

$$D = \lim_{t \to \infty} \frac{1}{6t} \langle |r(t) - r(0)|^2 \rangle, \qquad (24)$$

where $r(t)$ means the position vector of an ion at time t. Then the calculated diffusion constants for molten NaCl and experimental data[32] are shown in Fig. 10. The calculated results agree with the experimental data, the maximum error for cation is within $\pm 10\%$, and for anion is within $\pm 20\%$. This is mainly caused by that the calculated diffusion con-
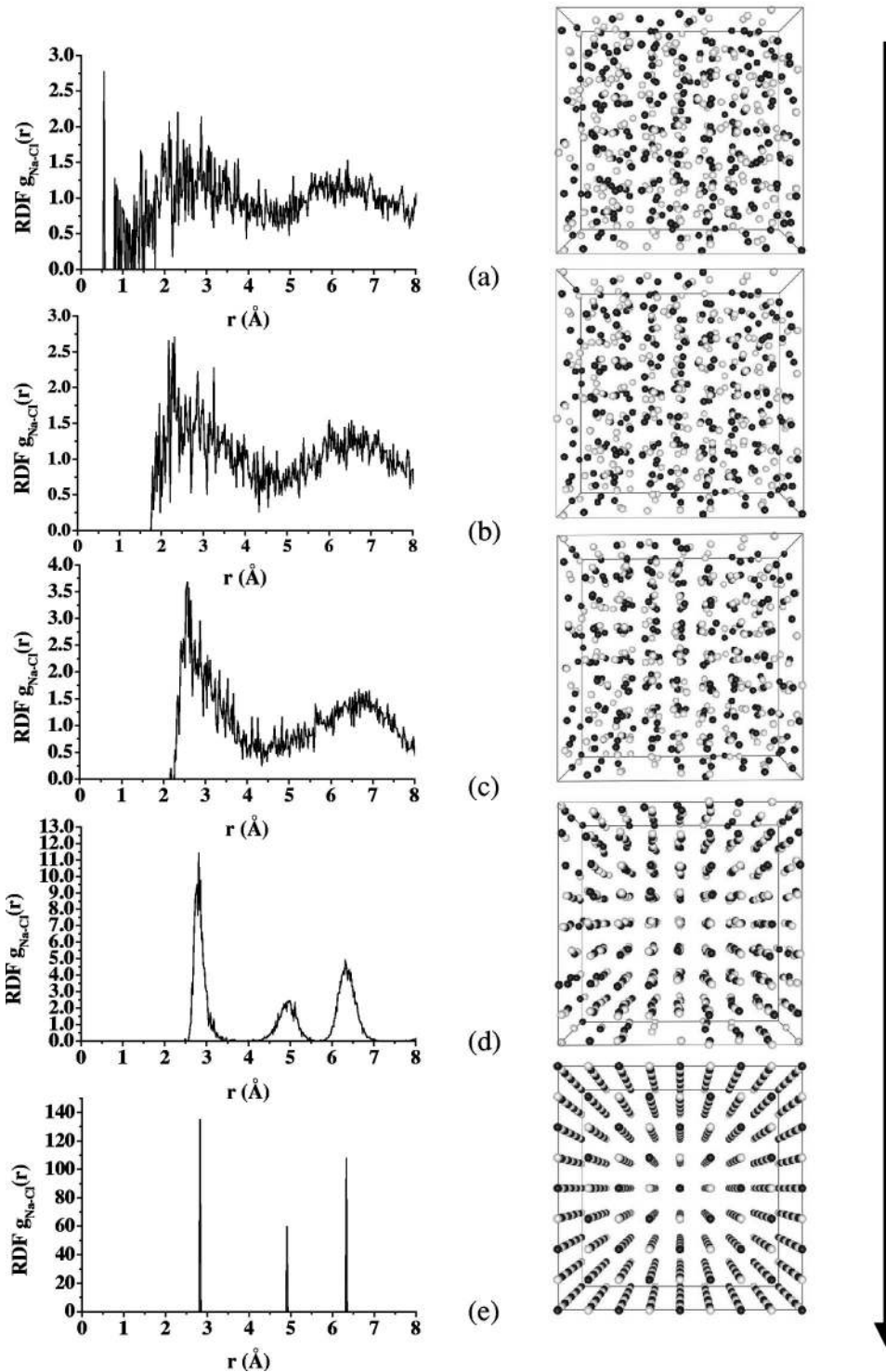
FIG. 6. Perspective configurations of the transition from disordered (a) to ordered NaCl (e), and the corresponding radial distribution function RDF's have also been shown.

stant for anion is closer to that for cation than the observed results. This seems that cation and anion take the similar motions in molten NaCl under the control of our potentials. This result is similar to the MD simulation of Koishi,[33] which was based on Tosi and Fumi's empirical potentials.[34]

V. DISCUSSION AND CONCLUSIONS

In the present work, the interionic pair potentials were derived from pseudopotential total energies with multiple-

lattice inversion techniques. And the total energies are not only from equilibrium position of the key structure $B1$, but also from nonequilibrium states and the other related virtual structures $B3$, $T1$, and $T2$, whose lattice constants cover from 4.5 to 10.0 Å, and even extended to 16.0 Å in $B1$- and $B3$-type NaCl. This scheme effectively extends the phase space of configurations beyond the equilibrium $B1$ structure, then provides more information on interionic interaction over a fair wide range of interionic separations. In fact, from $B1$ to its virtual structures, the nearest-neighbor coordination
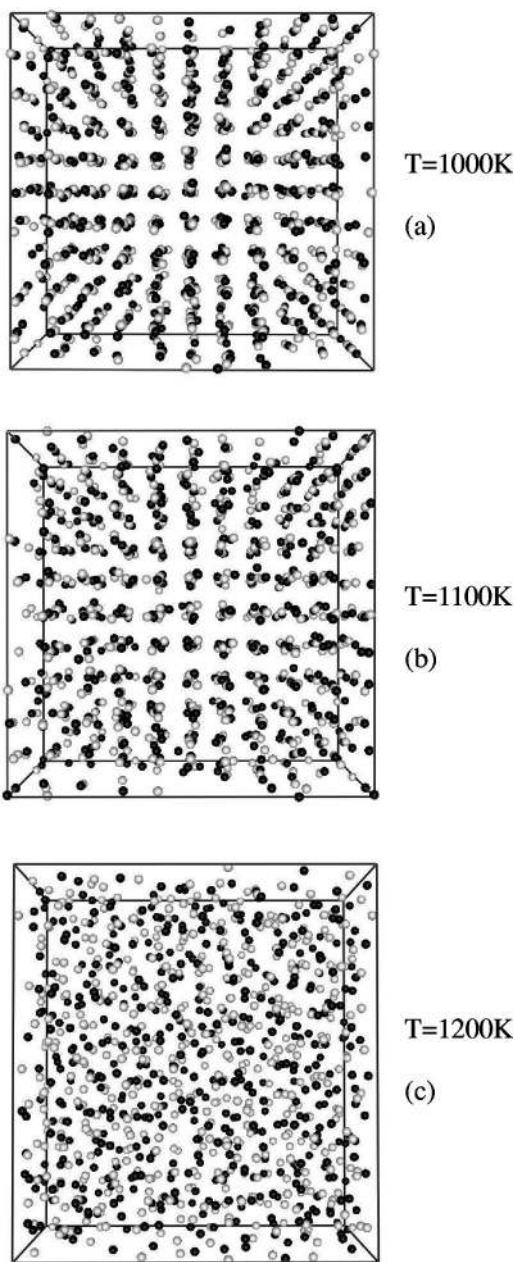
FIG. 7. Snapshot of perspective configurations around melting temperature after 15 000 time steps, (a) $T = 1000$ K, (b) $T = 1100$ K, and (c) $T = 1200$ K.

number varies from 6 to 4, and the bond angle changes from $90°$ to $109°28'$. Hence the interionic potentials of NaCl exhibit promising ability in the simulations for $B1$, $B2$, and disordered and molten NaCl.

Although the recent work of Fracchia[36] and Rodeja[8] also derived the interionic potentials from the extended phase space, the scheme in this work has two main features as follows. First, our interionic pair potentials cover much larger phase space including not only the $B1$ phase, but also $B3$ and two $P4/mmm$ structures with nonequilibrium states. In the previous work, the phase space was just extended a little beyond the equilibrium state. Second, this work is a parameter-free method to derive interionic potentials. The
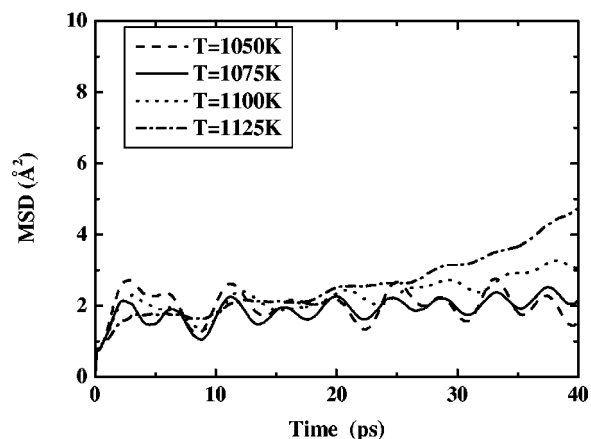

FIG. 8. The calculated mean-square displacements (MSD's) from 1050 to 1125 K.
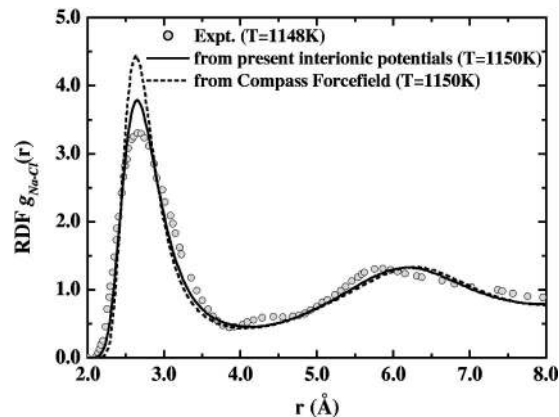

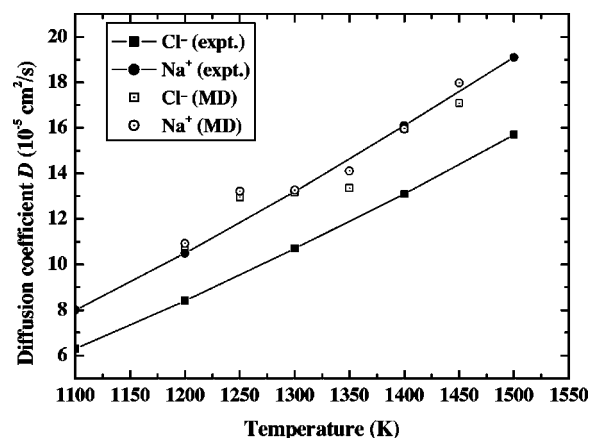FIG. 9. Radial distribution function $g_{Na\text{-}Cl}(r)$ for molten NaCl.

FIG. 10. The diffusion constants of molten NaCl.

potential functions could be selected in terms of the shapes of the inverted potential curves. However, both Fracchia and Rodeja had to use the *a priori* potential function forms with the adjustable potential parameters. This led to five sets of potential parameters obtained in Rodeja's work. Which set is the best had to be discussed according to their simulation results. Overall, combining the *ab initio* total-energy calculations and lattice inversion, our scheme seems to be more promising in derivation of interionic pair potentials for ionic solids.

Even though it is very difficult to summarize a rule about how to build effective virtual structures for different ionic solids, the difference between various structures is worth exploring for interionic potentials.

[1] J. Hafner, Acta Mater. **48**, 71 (2000).

[2] R. A. Jackson and K. A. Mort, Comput. Mater. Sci. **17**, 230 (2000).

[3] M. B. Taylor, G. D. Barrera, N. L. Allan, T. H. K. Barron, and W. C. Mackrodt, Comput. Phys. Commun. **109**, 135 (1998).

[4] N. L. Allan and W. C. Mackrodt, Philos. Mag. B **69**, 871 (1994).

[5] J. D. Gale, Philos. Mag. B **73**, 3 (1996).

[6] K. Ihata and H. Okazaki, J. Phys.: Condens. Matter **9**, 1477 (1997).

[7] J. H. Harding and D. J. Harris, Phys. Rev. B **60**, 2740 (1999).

[8] J. G. Rodeja, M. Meyer, and M. Hayoun, Modell. Simul. Mater. Sci. Eng. **9**, 81 (2000).

[9] J. D. Gale, C. R. A. Catlow, and W. C. Mackrodt, Modell. Simul. Mater. Sci. Eng. **1**, 73 (1992).

[10] J. A. Purton, D. M. Bird, S. C. Parker, and D. W. Bullett, J. Chem. Phys. **110**, 8090 (1999).

[11] C. R. A. Catlow, *Computer Modelling in Inorganic Crystallography* (Academic, London, 1997), pp. 56–59.

[12] M. C. Payne, I. J. Robertson, D. Thomson, and V. Heine, Philos. Mag. B **73**, 191 (1996).

[13] N. X. Chen, Z. D. Chen, and Y. C. Wei, Phys. Rev. E **55**, R5 (1997).

[14] N. X. Chen, X. J. Ge, W. Q. Zhang, and F. W. Zhu, Phys. Rev. B **57**, 14 203 (1998).

[15] V. Vitek, MRS Bull. **21** (2), 20 (1996).

[16] M. C. Payne, M. P. Teter, D. C. Allan, T. A. Arias, and J. D. Joannopoulos, Rev. Mod. Phys. **64**, 1045 (1992).

[17] CASTEP, Molecular Simulation Software, 1998.

[18] I. Yoji, M. Masakazu, and T. Tatsuo, Thin Solid Films **381**, 176 (2001).

[19] http://www.accelrys.com/cerius2/castep.html

[20] H. J. Monkhorst and J. D. Pack, Phys. Rev. B **13**, 5188 (1976).

[21] P. P. Ewald, Ann. Phys. (Leipzig) **64**, 253 (1921).

[22] J. M. Recio, E. Francisco, M. Flórez, and A. M. Pendás, J. Phys.: Condens. Matter **5**, 4975 (1993).

[23] M. J. L. Sangster, J. Phys. Chem. Solids **34**, 355 (1973).

[24] Z. Peng, C. S. Ewig, M-J. Hwang, M. Waldman, and A. T. Hagler, J. Phys. Chem. **101**, 7243 (1997).

[25] H. Zhang and M. S. T. Bukowinski, Phys. Rev. B **44**, 2495 (1991).

[26] A. J. Cohen and R. G. Gorden, Phys. Rev. B **12**, 3228 (1975).

[27] D. L. Heinz and R. Jeanloz, Phys. Rev. B **30**, 6045 (1984); Y. Sato-Sorensen, J. Geophys. Res. **88**, 3543 (1983).

[28] F. Lantelme, P. Turq, B. Quentrec, and J. W. E. Lewis, Mol. Phys. **28**, 1537 (1975).

[29] J. Shanker, M. P. Sharma, S. S. Kushwah, J. Phys. Chem. Solids **60**, 603 (1999).

[30] S. Melchionna, G. Ciccotti, and B. L. Holian, Mol. Phys. **78**, 533 (1993).

[31] M. Dixon and M. J. L. Sangster, J. Phys. C **9**, L5 (1976).

[32] J. W. E. Lewis, K. Singer, J. Chem. Soc., Faraday Trans. 2 **71**, 41 (1975).

[33] T. Koishi and S. Tamaki, J. Non-Cryst. Solids **250–252**, 501 (1999).

[34] M. P. Tosi and F. G. Fumi, J. Phys. Chem. Solids **25**, 45 (1964).

[35] J. W. E. Lewis and K. Singer, J. Chem. Soc., Faraday Trans. 2 **71**, 41 (1975).

[36] R. M. Fracchia, G. D. Barrera, N. L. Allen, T. H. K. Barron, and W. C. Mackrodt, J. Phys. Chem. Solids **59**, 435 (1998).